Evaluation of Tablet Formation of Different Lactoses by 3D Modeling and Fractal Analysis

Z. Jelcic
PLIVA-Research and
Development Ltd.,
Pharmaceutical Technology,
Prilaz baruna Filipovica,
Zagreb, Croatia

**K. Hauschild, M. Ogiermann
and K. M. Picker-Freyer**
Martin-Luther-University
Halle-Wittenberg, Institute of
Pharmaceutical Technology and
Biopharmacy, Halle/Saale,
Germany

ABSTRACT The aim of this study was to use 3D modeling to differentiate not only among the four different types of lactose α-lactose monohydrate, spray-dried lactose, agglomerated lactose and lactose anhydrous but also between products from different manufacturers. Further "box-counting" fractal analysis of SEM images was done to gain additional information on tableting characteristics and tablet properties which can be found in the fractal structure. Twelve different materials from different manufacturers were analyzed for their powder-technological and physicochemical properties. They were tableted on an eccentric tableting machine at graded maximum relative densities and the recorded data, namely force, time, and displacement were analyzed by the 3D modeling technique. Tablet properties such as, elastic recovery, crushing force and morphology were analyzed. The results show that 3D modeling can precisely distinguish deformation behavior for different types of lactose and also for the same type of material produced with a slightly different technique. Furthermore, the results showed that the amorphous content of the lactose determined the compactibility of the material, which is due to a reversible exceeding of the glass transition temperature of the material. The three fractal dimensions D_{BW} (box surface dimension), D_{WBW} (pore/void box mass dimension), and D_{BBW} (box solid mass dimension) are capable of describing morphological differences in lactose materials. Multivariate regression analysis showed that the fractal surface structure of the lactose-based materials is strongly correlated to tableting characteristics and tablet properties. Especially with regards to 3D modeling, it was found that the fractal indices can describe the parameters time plasticity d, pressure plasticity e, and fast elastic decompression, which is the inverse of ω. In addition, the 3D parameters are able to describe the powder and tablet fractal indices. In conclusion, the 3D modeling is not only able to characterize the compression process but it can also provide information on the final tablet morphology.

Address correspondence to
K. M. Picker-Freyer, Martin-Luther-
University Halle-Wittenberg, Institute
of Pharmaceutical Technology and
Biopharmacy, Wolfgang-Langenbeck-
Str. 4, 06120 Halle/Saale, Germany;
Tel: +49-345-552 5138; Fax: +49-345-
552 7029; E-mail: katharina.picker-
freyer@pharmazie.uni-halle.de

INTRODUCTION

In order to characterize tableting properties of direct compression materials rapidly and distinctly in one step, the 3D model was developed (Picker, 2000, 2003a). It is the only compression model which is based on all of the three important parameters necessary to characterize the tableting process namely force, time, and displacement. The 3D modeling technique has already been successful in differentiating between materials with different as well as with similar deformation mechanisms (Picker & Bikane, 2001; Picker, 2004). Furthermore, it is able to differentiate pressure dependent and time dependent deformation. The method has been experimentally tested for its explanatory power and applicability, especially the parameters can be traced back in experiments. Time plasticity d is influenced by speed, pressure plasticity d correlates with microhardness, and the twisting angle, an indicator for elasticity, correlated with the elastic modulus (Picker, 2002, 2003b). Furthermore, the results of 3D modeling have been validated by comparison with other well-established characterization techniques (Picker, 2002). In this study, the 3D modeling will be used to differentiate not only between the four lactose products–α-lactose-monohydrate, spray-dried lactose, agglomerated lactose, and lactose anhydrous but also between products of different manufacturers with slightly different properties.

Lactose is a major excipient in tablet manufacture and has been used for more than 50 years in tableting. It improves direct compression and over the years different types of lactose have been developed and studied extensively. The primary material crystalline α-lactose-monohydrate shows mainly fragmentation during tableting and its binding ability is low compared to other materials (e.g., Lerk, 1993). The follow up materials spray-dried lactose, agglomerated lactose, and lactose anhydrous show improved direct compression properties (e.g., Gunsel & Lachman, 1963; Bolhuis et al., 1985; Vromans et al., 1987; Bolhuis & Chowhan, 1996; Busignies et al., 2004).

Nowadays, these materials are produced by different manufacturers with slightly different production methods. Since the proprietary production processes of lactose are not generally known, it is possible to make only a few general statements on the subject:

α-lactose-monohydrate crystallizes below 93.5°C from supersaturated solutions of lactose. It can be prepared by special crystallization procedures using different cooling rates and steps. The resulting products not only differ in particle size, but they can also show compression characteristics which are improved or have worsened in quality.

Spray-dried lactose has been prepared according to a patented process since 1958 (Gunsel & Lachman, 1963). However, some process parameters such as spraying rate and temperature of the feed solution can be varied within a narrow range and each manufacturer has its own production method.

A huge difference in process parameters exists for the agglomerated lactoses since the granulation parameters can be widely varied.

The commercially available lactose anhydrous consists mainly of β-lactose and is usually prepared by roller drying. As for the other materials, the production procedure is the proprietary of the manufacturer and depends on his choice of conditions such as mechanical agitation and drying temperature.

Furthermore, it is possible to differentiate the products by their powder-technological and physicochemical properties as e.g., glass transition temperature, particle size, apparent particle density, and bulk and tap density. These properties influence the tableting process to a great extent.

In this study, special attention will be given to the morphology of the powders and tablets. Material surfaces contain information on the mechanism of surface generation (e.g., Tang et al., 2004). For example, the morphology of powders and more likely tablets keeps information on tableting performance, tableting characteristics and final tablet properties (Podczeck et al., 1999). Thus, scanning electron microscopy (SEM) allows for a qualitative approach to surface topography and is a morphological approach to surface roughness as well.

During the last decades, several authors have tried to quantify the surface roughness of materials by image analysis (Underwood & Banerji, 1983). When an object has a homogeneous composition, an image of its surface is known to be directly related to the real

relief of its surface (Blacher et al., 1997). In this study, we used fractal analysis of SEM images to characterize the surface roughness of pharmaceutical solid materials. The aim of this study was to gain additional information on tableting characteristics and tablet properties which can be found in the fractal surface structure. From the morphology by fractal analysis, (a non-integer number), the fractal index will be derived; this analysis allows to compare the properties of the lactoses and lactose tablets to each other. The properties of the lactoses analyzed and correlated with the fractal index in this study are the Carr-index, the parameters of 3D modeling, namely time plasticity, pressure plasticity, and fast elastic decompression. The properties of the lactose tablets analyzed and correlated to the fractal index are elastic recovery and crushing force. The inverse problem which means the derivation of fractal indices from the 3D-model parameters will also be evaluated.

Theoretical Background: Fractals

The concept of fractals (Mandelbrot, 1982; Frame et al., 2006) has been used in various scientific fields and is a new tool that is already being applied to pharmaceutical science (see an excellent review by Tang et al., 2004).

The fractal analysis has already been used to characterize particle morphology (Concessio & Hickey, 1997) or flow characteristics (Hickey & Concessio, 1994). The morphological and surface characteristics by fractal dimensions of lactose and coated lactose powder particles were investigated in interactive mixtures used in dry powder inhalers (Holgado et al., 1995; Bower et al., 1995; Ferrari et al., 2004). Fractals are qualitatively characterized by their "roughness" (nondifferentiability) and their "self-similarity". Quantitatively, the amount of variation in the structure or surfaces of a fractal object can be described with a number D_F, called the fractal dimension, which is a measure of the texture, or fragmentation, of the object.

The surfaces of most materials are fractals, that is, at this range, surface geometric irregularities and defects are characteristically self-similar upon variations of resolution (Avnir et al., 1984). Smooth surfaces have a low fractal dimension, and highly textured surfaces have a high fractal dimension. The fractal nature of powder systems is well established (Kaye, 1995) and fractals can

be used to describe quite variable powder particle systems (Fini et al., 1996, 1997). Thus, the fractal dimension is a useful tool for classifying powder particle features in SEM imagery (Chappard et al., 2003).

By variations in the processing the surfaces and surface texture of lactose can be modified, which influences the performance of the final dosage form in many different levels. Surface texture has an effect on the properties of powders and tablets (Seitavuopio et al., 2003, 2005). Compression pressure during tablet compaction influences the surface texture of the compacts. Several researchers have showed this over the years (Rowe, 1979; Riippi et al., 1998; Podczeck et al., 1999; Khan et al., 2001). At lower compression pressures, tablet surfaces can have characteristic peaks and valleys which originate from the initial powder particle morphology (Podczeck, 1998). At higher compression pressures, the voids between the particles close up and the surface becomes smoother. The type and amount of excipients also affect the surface texture of the tablets (Narayan & Hancock, 2005). In addition to the role that fractal geometry has in the quantification of the particle structure, it can also be used to address the relation between structure and a range of physical processes occurring in the compacts. This ability to directly relate structure to function is one of the most important and beneficial features of fractal models.

EXPERIMENTAL PART
Materials

The excipients analyzed were three types of α-lactose monohydrate (LM, abbreviations: LM 1, LM 2a, LM 2b), four agglomerated lactoses (AGL, abbreviations: AGL 1a, AGL 1b, AGL 2, and AGL 3), two types of lactose anhydrous (LA, abbreviations: LA 1 and LA 3), and three spray-dried lactoses (SL, abbreviations: SL 1, SL 2, and SL 3). 1, 2, and 3 are abbreviations for three different manufacturers.

Methods
Test Conditions

All materials and tablets were equilibrated, produced and stored at 45% RH. Tableting was performed in a special climate-controlled room which was set to $23 \pm 1°C$ and $45 \pm 2\%$ RH.

Lactoses by 3D Modeling and Fractal Analysis

Glass Transition Temperature

The glass transition temperature T_g of the dry material was determined using DSC 200 (Netzsch Gerätebau GmbH, Selb, Germany) during the first heating. Sample size varied in between 5 and 10 mg. The heating rate was 40 K min⁻¹. Only with a high heating rate weak transitions can be determined (Picker, 2003c). The temperature interval was set to 20 to 150°C. The T_g was determined by calculating the temperature of the half step height. To verify the results the maximum of the first derivative was also determined.

Crystallinity

The crystallinity of the powders was determined using a Roentgen diffractometer (URD 63, Freiberger Präzisionsmechanik, Freiberg, Germany). The radiation was copper and a nickel filter was used. Bragg's angle was analyzed between 3 and 50 2Θ.

Particle Size

Particle size distribution was determined by sieve analysis according to DIN 66165 (Retsch sieving machine, Type Vibrio, No. 12189031, Retsch GmbH and Co. KG, Haan, Germany) in triplicate. The mean particle size distribution was calculated and median particle size of this distribution was determined.

Densities

The apparent particle density of all of the materials was determined by Helium pycnometry (Accupyc 1330, Micromeritics, Norcross, GA) in triplicate. The equilibrated materials were analyzed in order to determine the apparent particle density of the materials containing some moisture.

Bulk and tap density were determined with two repetitions in a weighed 250 mL cylinder using a volumeter (Erweka GmbH, Heusenstamm, Germany). A total of 100 g of the powder was gently filled into the cylinder. The bulk volume was read and bulk density was calculated. Afterwards the cylinder was tapped at least 2500 times up to constant volume. Tap volume was read and tap density calculated. Mean and standard deviations were determined.

Flowability

To analyze flowability, the parameter Carr-index (Carr, 1965) was calculated using the following equation:

$$
\text{Carr} - \text{index} = \text{compressibility}[\%]
$$
$$
= \frac{\text{tapdensity} - \text{bulkdensity}}{\text{tapdensity}} \cdot 100 \quad (1)
$$

Tableting

The powder was mixed with 0.5% (v/v) magnesium stearate for 5 min at level 6 in a cubic mixer (ERWEKA, Heusenstamm, Germany) prior to tableting.

Tablets were produced on an instrumented eccentric tableting machine (Korsch EK0, Korsch Maschinenfabrik, Berlin, Germany) with 11-mm flat-faced punches (Ritter GmbH, Berlin, Germany). Tablets were produced at five graded different maximum relative densities ($\rho_{rel,max}$, precision 0.001): 0.77, 0.81, 0.85, and 0.88. The relative density is the quotient of the density of the tablet to the apparent particle density. The minimum tablet height under load was always 3 mm. Displacement of the punch faces was measured using an inductive transducer (W20 TK, Hottinger Baldwin Meßtechnik, Darmstadt, Germany) and corrected for elastic deformation of the punches. The depth of filling was held constant at 13 mm. The production rate was 10 tablets/min. The amount of material necessary for each tablet with a given $\rho_{rel,max}$ was calculated. The powder was manually filled into the die, and one compaction cycle was performed. Ten single tablets were produced at each condition.

Data acquisition was performed by a DMC-plus system (Hottinger Baldwin Meßtechnik, Darmstadt, Germany) with a rate of 600 Hz, and data were stored by BEAM-Software (AMS-Flöha, Germany). Force, time, and displacement of the upper punch were recorded for each compaction cycle. Normalized time, pressure, and ln (1/1 – D_{rel}) according to Heckel (Heckel, 1961) were calculated for five compaction cycles of each material. Only data > 1 MPa were used for analysis.

3D Modeling

For applying the 3D modeling technique (Picker, 2003a), all three measured values were presented in a 3D data plot. To this 3D data plot, a twisted plane was fitted by the least-squares method according to Levenberg-Marquard (Matlab$^{®}$) with the following equation. The plane is twisted at $t = t_{max}$.

$$z = \ln\left(\frac{1}{1 - D_{rel}}\right) = ((t - t_{max}) \cdot (d + \omega \cdot p_{max} - p))$$
$$+ (e \cdot p) + (f + d \cdot t_{max}) \qquad (2)$$

where D_{rel} indicates relative density; t, normalized time; t_{max}, time at maximum pressure; p_{max}, maximum pressure; d, time plasticity; e, pressure plasticity; f, intersection; p, pressure; and ω, fast elastic decompression (angle of torsion).

The parameters of the fitted plane, $d, e,$ and ω, of the five compaction cycles at each tableting condition (material at a given $\rho_{rel,max}$) were averaged, and means and standard deviations were calculated (Table 1). These parameters were exhibited in the 3D-parameter plot.

Time plasticity d describes the plastic deformation of the excipient according to time. Tableting speed can influence it (Picker, 2003b). Pressure plasticity e describes the relationship between density and pressure. With increasing pressure plasticity e the necessary pressure for deformation decreases. The fast elastic decompression ω is a measure of the material's elasticity. The elasticity decreases when ω increases (Picker, 2004).

Elastic Recovery

The axial elastic recovery was determined by a micrometer screw (Mitutoyo, Tokyo, Japan). Ten tablets were analyzed, and the means and standard deviations were calculated.

Elastic recovery was calculated using the following equation (Armstrong and Haines-Nutt, 1972):

$$ER\,(\%) = 100\,\frac{H_1 - H_0}{H_0} \qquad (3)$$

with ER = elastic recovery, H_1 = height of the tablet at a certain time after tableting, and H_0 = minimal height of tablet under load.

The calibrated inductive transducer (W 20 TK, Hottinger Baldwin Meßtechnik, Darmstadt, Germany) was used to measure the position of the upper punch and thus the axial expansion in the die.

In addition, elastic recovery was exemplarily determined dependent on time. For this purpose, directly after tableting out-die measurements were performed. Thermo mechanical analysis (TMA, Netzsch Gerätebau GmbH, Selb, Germany; precision: 0.0005–0.001 mm) was used to measure the height changes continuously (Picker, 2002).

Crushing Force

The radial crushing force of the tablets was determined with 2.3 mm/s rate of compression during the crushing force test (TBH 30, Erweka GmbH, Heusenstamm Germany). Five tablets were analyzed 10 days after tableting, and the means and standard deviations were calculated.

Scanning Electron Microscopy

The surface of both powder and tablets was analyzed by scanning electron microscopy (SEM) (JSM 6400, JEOL, Tokyo, Japan) at an accelerating voltage of 5 keV. Before the analysis they were mounted onto a sample holder and coated with coal/gold/coal (Balzer, Liechtenstein, Type SCD 050).

Fractal Analysis

Fractal dimension values were computed for the microscopic fine-sized texture in the SEM images of lactose powder particles and of tablet surfaces. The Adobe Photoshop 7.0 software and Scion software (http://www.scioncorp.com/index.htm) were selected for image processing, and HarFa software (http://www.fch.vutbr.cz/lectures/imagesci/harfa.htm) for the fractal analysis by a "box-counting" method. We consider a binary, thresholded SEM image as displaying fractal landscape of two phases—solid and pore (or void). The box-counting method is based on a simple principle (Buchníček et al., 2000) where a square mesh of various sizes $1/\varepsilon$ is laid over the image object. Mesh boxes N_{BBW} (ε) that contain any part of the boxes which cover the solid phase fractal are counted (e.g., squares which are completely filled up by the fractal N_B and squares which contain just part of fractal N_{BW} are added). For a fractal set, the number of boxes N

Lactoses by 3D Modeling and Fractal Analysis

TABLE 1 Parameters of the 3D Model (Mean ± SD)

Material	$\rho_{rel, max}$	d	e (MPa^{-1})	ω
LM 1	0.88	0.7915 ± 0.0023	0.0038 ± 0.0001	0.0070 ± 0.0001
	0.85	0.7211 ± 0.0074	0.0038 ± 0.0001	0.0064 ± 0.0001
	0.81	0.3877 ± 0.0143	0.0045 ± 0.0000	0.0118 ± 0.0004
	0.77	0.2858 ± 0.0150	0.0055 ± 0.0000	0.0152 ± 0.0002
LM 2a	0.88	0.8055 ± 0.0048	0.0037 ± 0.0001	0.0063 ± 0.0000
	0.85	0.5934 ± 0.0034	0.0039 ± 0.0001	0.0085 ± 0.0001
	0.81	0.4483 ± 0.0188	0.0048 ± 0.0001	0.0117 ± 0.0007
	0.77	0.3236 ± 0.0022	0.0057 ± 0.0002	0.0144 ± 0.0004
LM 2b	0.88	0.8449 ± 0.0031	0.0037 ± 0.0000	0.0071 ± 0.0000
	0.85	0.6310 ± 0.0059	0.0039 ± 0.0000	0.0097 ± 0.0001
	0.81	0.4850 ± 0.0021	0.0042 ± 0.0000	0.0128 ± 0.0001
	0.77	0.3955 ± 0.0038	0.0056 ± 0.0001	0.0180 ± 0.0002
AGL 1a	0.88	0.6533 ± 0.0044	0.0032 ± 0.0001	0.0055 ± 0.0001
	0.85	0.4812 ± 0.0040	0.0034 ± 0.0001	0.0070 ± 0.0002
	0.81	0.3297 ± 0.0019	0.0040 ± 0.0001	0.0090 ± 0.0001
	0.77	0.2357 ± 0.0013	0.0048 ± 0.0000	0.0121 ± 0.0002
AGL 1b	0.88	0.5645 ± 0.0022	0.0028 ± 0.0000	0.0042 ± 0.0001
	0.85	0.3971 ± 0.0019	0.0031 ± 0.0001	0.0058 ± 0.0001
	0.81	0.3092 ± 0.0023	0.0036 ± 0.0001	0.0083 ± 0.0002
	0.77	0.2125 ± 0.0020	0.0046 ± 0.0001	0.0117 ± 0.0002
AGL 2	0.88	0.7945 ± 0.0079	0.0030 ± 0.0001	0.0053 ± 0.0001
	0.85	0.5645 ± 0.0085	0.0033 ± 0.0001	0.0070 ± 0.0001
	0.81	0.4203 ± 0.0023	0.0036 ± 0.0001	0.0095 ± 0.0001
	0.77	0.3150 ± 0.0020	0.0039 ± 0.0000	0.0131 ± 0.0002
AGL 3	0.88	0.9345 ± 0.0050	0.0022 ± 0.0000	0.0054 ± 0.0000
	0.85	0.6393 ± 0.0039	0.0026 ± 0.0000	0.0066 ± 0.0001
	0.81	0.4256 ± 0.0051	0.0031 ± 0.0000	0.0092 ± 0.0001
	0.77	0.3120 ± 0.0031	0.0038 ± 0.0000	0.0120 ± 0.0001
LA 1	0.88	0.7630 ± 0.0051	0.0020 ± 0.0000	0.0056 ± 0.0001
	0.85	0.4716 ± 0.0019	0.0026 ± 0.0000	0.0061 ± 0.0000
	0.81	0.3109 ± 0.0022	0.0030 ± 0.0001	0.0084 ± 0.0000
	0.77	0.2062 ± 0.0035	0.0039 ± 0.0001	0.0120 ± 0.0002
LA 3	0.88	0.7983 ± 0.0067	0.0021 ± 0.0000	0.0042 ± 0.0000
	0.85	0.5174 ± 0.0017	0.0024 ± 0.0000	0.0048 ± 0.0000
	0.81	0.3480 ± 0.0023	0.0026 ± 0.0000	0.0067 ± 0.0001
	0.77	0.2304 ± 0.0010	0.0031 ± 0.0000	0.0091 ± 0.0001
SL 1	0.88	0.8967 ± 0.0258	0.0027 ± 0.0001	0.0062 ± 0.0002
	0.85	0.6995 ± 0.0056	0.0029 ± 0.0000	0.0076 ± 0.0001
	0.81	0.5425 ± 0.0049	0.0031 ± 0.0001	0.0092 ± 0.0001
	0.77	0.4091 ± 0.0126	0.0035 ± 0.0001	0.0109 ± 0.0003
SL 2	0.88	0.8978 ± 0.0071	0.0029 ± 0.0000	0.0047 ± 0.0000
	0.85	0.6660 ± 0.0044	0.0030 ± 0.0000	0.0063 ± 0.0000
	0.81	0.5137 ± 0.0067	0.0032 ± 0.0000	0.0080 ± 0.0000
	0.77	0.3908 ± 0.0027	0.0035 ± 0.0001	0.0100 ± 0.0001
SL 3	0.88	0.9353 ± 0.0081	0.0022 ± 0.0000	0.0052 ± 0.0001
	0.85	0.6998 ± 0.0025	0.0028 ± 0.0000	0.0063 ± 0.0000
	0.81	0.4841 ± 0.0018	0.0032 ± 0.0000	0.0077 ± 0.0001
	0.77	0.3561 ± 0.0032	0.0033 ± 0.0000	0.0091 ± 0.0001

$(1/\varepsilon)$ satisfies the relation, $N(1/\varepsilon) \sim (1/\varepsilon)^{-D}$, where D is the mass fractal dimension. Dimension D_{BBW} is referred to as a "classical" box dimension. Counting black, white and partially black squares separately can modify this method. Three new fractal dimensions D_B, D_W, and D_{BW} can be obtained. D_B and D_W

Z. Jelcic et al.

characterize fractal properties of the black and white plane, while D_{BW} characterizes properties of the black and white boundary. The fractal nature of lactose particles and tablets has been studied at two distinct levels using the measures of the surface/ border fractal dimension (D_{BW}), effectively allowing discrimination between systems which are only fractal at their boundaries, and the two box-counting mass fractal dimensions, applicable in cases where the interior of the system has gaps (a measure of the solid D_{BBW}, and void (or pore) D_{WBW} space-filling capacity of the interior). The pore (or void) fractal index D_{WBW} (arises by adding squares N_W that do not contain fractals and remaining white and squares N_{BW} that contain just boundary part of fractals). Powder particle can be a fractal as a dense object with a fractal surface. The smallest from the trinity of dimensions, the surface fractal index $D_{BW,powder}$ characterizes the properties of the border or the surface of the fractal powder particles.. The solid mass fractal index $D_{BBW,powder}$ characterizes the solid properties of the powder particle structure. However, the compacted tablet can be fractal as a mass fractal (a cluster or a network) and as a pore fractal (a dense object with porosity). Two box-counting, capacity or mass fractal dimensions can be estimated for each image, and used to describe the space-filling ability of solid ($D_{BBW,tablet}$) and pore ($D_{WBW,tablet}$) networks, respectively. The surface fractal index D_{BW} characterized the properties of the border of black and white color, i.e., the interface of the solid and pore objects in the SEM image. The values of D are always less than two, since two would be expected for a completely filled rectangle.

The fractal dimension determination protocol, the box-counting method, was validated by comparing the calculated and theoretical fractal dimension D_{true} of known ideal, mathematical fractals (von Koch snow flakes, von Koch island, Sierpinski gasket and Sierpinski carpet, and Euclidian form of solid black square). The "true" fractal dimensions are statistically significant and positively correlated with the solid D_{BBW} ($F_{signif}(1,3) = 0.0002$) and surface D_{BW} ($F_{signif}(1,2) = 0.008$) fractal indices.

Topological Analysis

A thinning (or edge detection) algorithm was applied to the binary image to create an image containing only the image "skeleton", representing the

pixels in each pixel group that are essential for communicating the shape of the given pixel group. The thinning relates to the minimal structure of the image, and it can also be used for describing roughness, elongation of the object.

Thinning of the raster image to a single pixel width lines was performed as a multiclass segmentation in a gray level domain according to the Stentiford (Stentiford & Mortimer, 1983) algorithm in order to make the complex nature of the powder or tablet matrix observable. This edge thinning algorithm reduces edge to unit thickness while maintaining connectedness of the original pattern and eliminating local noise. The binary skeleton was further processed to identify fractal indices of branching points (the nodes where branches meet) and internal holes (the empty regions). The fractal dimension is directly proportional to the width of the contour line (Ahammer & DeVaney, 2004). In binary images, the pore–solid interface may be represented by a contour line with a thickness of 1 pixel. Hence, we are dealing with length fractals, and the obtained fractal dimension $D_{Stentiford}$ is expected to show values of $1 < D_{Stentiford} < 2$.

The effect of thinning on the fractal indices was tested for simple objects, such as a binary image of vase, ellipse, triangle, and H-letter (white objects on black background). The fractal indices D_{BW} and D_{WBW} are well correlated with that of thinned object (R = 0.907 and R = −0.957, respectively); and the D_{BBW} is only well correlated with the fractal index $D_{WBW,Stentiford}$ of the thinned object (R = 0.954). The Stentiford thinning method is applied also for the measurement of the fractal dimension of the particle-pore interface of the lactose particles and compacts.

Statistical Analysis

In order to compare the effects of different parameters further, a multivariate linear regression, based on the least squares method, among the variables was performed using a statistical analysis software (Statgraphics plus for Windows version 2.1, Manugistics, Rockville) and an Excel (Windows, Microsoft) add-in, Essential Regression (http://home.t-online.de/home/jowerner98/download.htm). Multivariate analyses were performed using a backward stepwise selection procedure: (1) all covariates and linear, interaction terms; (2) backward selection using a p-value cutoff of <0.1; and (3) best subset selection, with significant

Lactoses by 3D Modeling and Fractal Analysis

terms, high and significant coefficient of multiple correlation |R| ($p = 0.05$), and overall regression model significance $F_{signif}(k, n–k–1)$ (where n is the number of data points, and k the number of variables in the multiple regression model) below <0.05, that implies that there is a statistically significant relationship between the variables at the 95% or higher confidence level. A value of F_{signif} between 0.05 and 0.10 is considered marginally significant. The significance of the coefficient of multiple correlation |R|, was checked by the critical values of the for a two-tailed test ($p = 0.05$; df $= n – 2$; http://www-micro.msb.le.ac.uk/1010/rtable.html). Only regression models with the significant coefficient of multiple correlation |R| are reported in tables. Since the Durbin-Watson (DW) statistic tests value, for all presented regression models, is greater than 1.4, there is probably not any serious autocorrelation in the residuals.

RESULTS AND DISCUSSION
Material Properties

Physicochemical properties such as crystallinity and glass transition temperature are known to determine the deformation behavior of materials. Crystallinity was determined for the three materials consisting of α-lactose monohydrate. Fig. 1 exhibits that crystallinity increases in the following order SL
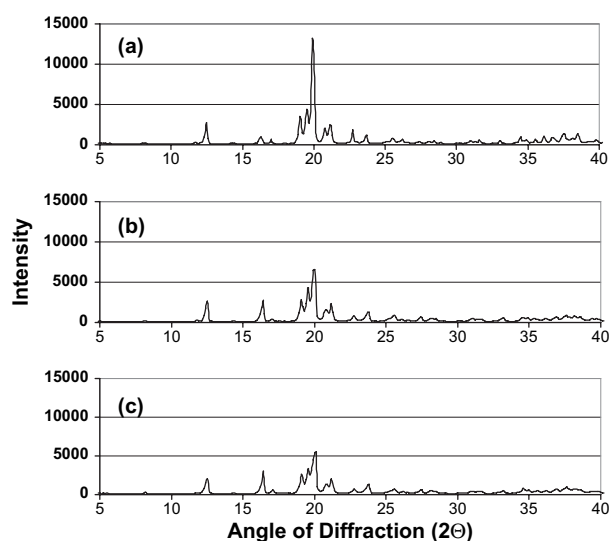
FIGURE 1 X-ray Diffractograms of (a) Crystalline α-Lactose Monohydrate, (b) Agglomerated Lactose, and (c) Spray-Dried Lactose.

< AGL < LM. The peak at 19.89 2θ was used for differentiation. LA which mainly contains β-lactose and thus possesses a different crystal structure was not included in analysis. T_g is dependent on the crystallinity and the amorphous content of the material. Only the amorphous parts of lactose can undergo a glass transition at a certain temperature. T_g determination was performed for all of the lactose types. However, only for SL, with the highest amorphous content, could a T_g be determined. The mean value was $75.0 \pm 5.6°C$. The differences for materials of different manufacturers fell in between standard deviation. Our result was in agreement with results in literature (Sebhatu et al., 1997).

In addition to the physicochemical properties, the powder-technological properties of different lactoses were analyzed. Median particle size, apparent particle density, bulk and tap density, and the Carr-index are given in Table 2. As what was to be generally expected differences between products from different manufacturers were much lower than differences between the four types of lactose. Here only the Carr-index will be discussed in more detail. The Carr-index C increases in the following order: AGL 1b > AGL 1a > LA 1 > AGL 2 = LA 3 = SL 1 > SL 2 > LM 2b = AGL 3 = LM 1 = SL 3 > LM 2a.

This means that the products of manufacturer 1 except for LM show generally worse flow properties which seem not to depend on the type of lactose. Moreover, it can also be stated that LA shows worse flow properties than the other materials. The other materials with a Carr-index below 14 show excellent (value 5–10) or almost excellent (good = value 12–16) flowability. The best flowing materials produced by spray-drying or agglomeration was indicated for manufacturer 3.

Tableting and tablet properties

Generally lactose is a material which deforms by brittle fracture accompanied by plastic deformation. The deformation of one type of LM and one type of SL have previously been described by 3D modeling (Picker, 2003a, 2004).

In the following, general differences between the types of lactose will be discussed followed by differences among the products of different manufacturers.

TABLE 2 Powder, Tableting Properties and Tablet Properties of Different Lactoses (Mean ± SD). Tablets were Produced at $\rho_{rel,\,max}$ of 0.88

Material	Median particle size (μm)	Apparent particle density (g/cm³)	Bulk density (g/cm³)	Tap density (g/cm³)	Carr-index (%)	Time plasticity d	Pressure plasticity e (Mpa⁻¹)	Twisting angle ω	Elastic recovery (%)	Crushing force (N)
LM 1	60	1.541 ± 0.000	0.716 ± 0.003	0.820 ± 0.007	12.7 ± 1.0	0.7915 ± 0.0023	0.0038 ± 0.0001	0.0070 ± 0.0001	3.7 ± 0.2	19.8 ± 1.3
LM 2a	100	1.540 ± 0.000	0.596 ± 0.000	0.671 ± 0.005	11.4 ± 0.6	0.8055 ± 0.0048	0.0037 ± 0.0001	0.0063 ± 0.0000	3.3 ± 0.2	30.7 ± 2.9
LM 2b	60	1.536 ± 0.001	0.730 ± 0.002	0.839 ± 0.005	13.0 ± 0.3	0.8449 ± 0.0031	0.0037 ± 0.0000	0.0071 ± 0.0000	3.6 ± 0.3	24.4 ± 1.3
AGL 1a	60	1.544 ± 0.001	0.579 ± 0.019	0.774 ± 0.018	25.1 ± 1.0	0.6533 ± 0.0044	0.0032 ± 0.0001	0.0055 ± 0.0001	2.3 ± 0.2	36.6 ± 2.0
AGL 1b	80	1.544 ± 0.002	0.552 ± 0.005	0.758 ± 0.008	27.2 ± 1.0	0.5645 ± 0.0019	0.0028 ± 0.0001	0.0042 ± 0.0001	2.0 ± 0.1	45.8 ± 1.3
AGL 2	100	1.548 ± 0.001	0.587 ± 0.004	0.697 ± 0.004	15.8 ± 1.3	0.7945 ± 0.0079	0.0030 ± 0.0001	0.0053 ± 0.0001	2.1 ± 0.3	33.8 ± 4.0
AGL 3	140	1.553 ± 0.001	0.555 ± 0.003	0.680 ± 0.005	12.9 ± 0.9	0.9345 ± 0.0050	0.0022 ± 0.0000	0.0054 ± 0.0000	2.4 ± 0.3	138.2 ± 1.9
LA 1	150	1.596 ± 0.002	0.660 ± 0.014	0.861 ± 0.011	23.3 ± 1.2	0.7630 ± 0.0051	0.0020 ± 0.0000	0.0056 ± 0.0001	3.3 ± 0.3	182.0 ± 6.1
LA 3	150	1.593 ± 0.003	0.702 ± 0.010	0.859 ± 0.008	15.7 ± 1.1	0.7983 ± 0.0067	0.0021 ± 0.0000	0.0040 ± 0.0000	2.8 ± 0.5	167.6 ± 7.3
SL 1	120	1.557 ± 0.003	0.570 ± 0.004	0.696 ± 0.003	18.1 ± 0.8	0.8967 ± 0.0258	0.0027 ± 0.0001	0.0062 ± 0.0002	3.2 ± 0.8	62.8 ± 3.1
SL 2	120	1.553 ± 0.001	0.622 ± 0.003	0.730 ± 0.003	14.8 ± 2.4	0.8978 ± 0.0071	0.0029 ± 0.0000	0.0047 ± 0.0000	3.1 ± 0.4	86.2 ± 11.6
SL 3	110	1.557 ± 0.002	0.651 ± 0.004	0.744 ± 0.002	12.6 ± 1.3	0.9353 ± 0.0081	0.0022 ± 0.0000	0.0050 ± 0.0001	3.1 ± 0.2	144.8 ± 6.4
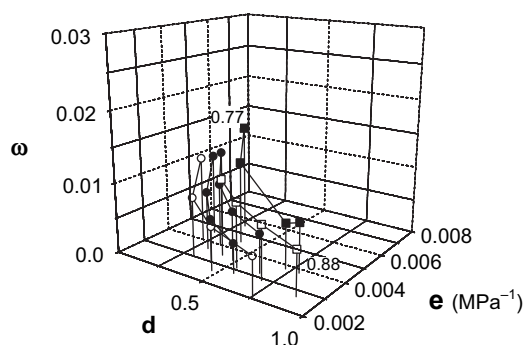
(a)
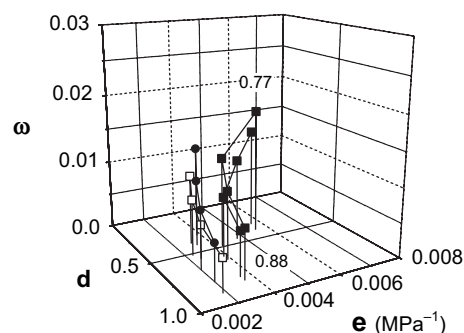
(b)
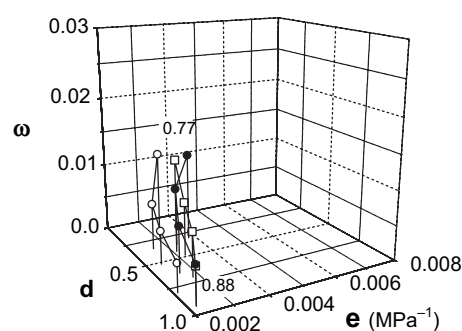
(c)

FIGURE 2 3D-Parameter Plot in Dependence on $\rho_{rel,\,max}$ (0.77–0.88) of ■ α-Lactose Monohydrate, ● Agglomerated Lactose, □ Spray-Dried Lactose, and ○ Lactose Anhydrous of Three Different Manufacturers (a), (b), and (c).

Comparison of Lactoses with Special Respect to the Type of Lactose

Fig. 2 and Table 1 exhibit the compression behavior of the different lactoses as characterized by 3D modeling. When viewed separately for each manufacturer, time plasticity *d* is the highest for SL and the lowest for LA and AGL. This means that SL with the highest *d*-values is the material which deforms the quickest.

The amorphous parts in SL might be responsible for this behavior.

Furthermore, LM shows the highest and LA the lowest pressure plasticity *e*. The pressure plasticity *e* increases in the following order: LA < SL ≤ AGL < LM. Hence, we can conclude that, the lowest pressure is needed for LM. This result is in accordance with results from Busignies et al. (2004) who claimed, based on Heckel analysis, that LM is the most ductile material. Other authors have established that the fracturing of the LM crystals is the predominant deformation mechanism for LM (e.g., Lerk, 1993). And LA requires the highest pressure since it has another crystal structure.

The elasticity according to the inverse of the angle of torsion ω is lower for LM than for all other types of lactose. Furthermore, ω strongly decreases for this material, which indicates brittle fracture for LM. Only brittle materials show a decrease in ω-values in the 3D parameter plots. The value of ω decreases a little less for AGL, and for LA and SL the plots are more flat, which indicates less fracture and a more homogenous deformation mechanism (Picker, 2004). In summation, brittle fracture decreases as follows: LM > AGL > LA > SL. In comparison, microcrystalline cellulose (Picker, 2003a) shows a very flat plot and a homogeneous deformation mechanism at all stages of densification.

The increase in plastic deformation and the decrease in brittle fracture from LM over AGL to SL correlate with the decrease in crystallinity as determined by X-ray-diffraction (Fig. 1). SL contains 15–20% amorphous lactose (Bolhuis & Chowhan, 1996). This amorphous material can undergo a glass transition and the temperature of this transition was determined as described above. The determined T_g is about 50 K higher than room temperature. Since during tableting temperature can increase between 35 K (e.g., Hanus & King, 1968) and 70 K (Schmidt, 1997) a reversible exceeding of the T_g during tableting is possible (Picker, 2003c). This transition from the glassy to the rubbery state and inverse must lead to good bonding in the final tablet (Picker-Freyer & Schmidt, 2004). A crystallization of the amorphous lactose might be induced.

The tablet properties of the different types of lactose will only be mentioned (Table 2), since they have been known for a long time. Generally, LM tablets showed the highest axial elastic recovery and tablets made of AGL the lowest. LA tablets had a similar elastic recovery when compared with SL tablets. The

crushing force of LM tablets was the lowest, and that of LA tablets the highest. For the materials based on α-lactose monohydrate tablets produced by SL exhibited the highest compactibility. This might be caused by the amorphous content which can contribute to bonding by a reversible exceeding of the glass transition temperature (Picker-Freyer & Schmidt, 2004).

Comparison of Lactoses with Special Attention given to the Manufacturer

Fig. 3a exhibits the compression behavior of three types of LM. Pressure plasticity e is similar at higher and also at low densification. For materials from the same manufacturer (manufacturer 2), time plasticity d is higher at lower particle size (LM 2b) and lower at higher particle size (LM 2a). ω is at all $\rho_{rel,max}$ lower for the material with a higher particle size. After tableting, a lower elastic recovery and a higher crushing force can be found for LM 2a with the higher particle size (Table 2). Interestingly, the product of the other manufacturer (LM 1) has d and ω-values more similar to LM 2a even when the particle size is different.

Fig. 3b gives the results for four types of AGL. In this case, e, d, and ω are lower for the material with the higher particle size (AGL 1b) than for the material with the lower particle size (AGL 1a) from the same manufacturer. In addition, a lower elastic recovery after tableting and a higher crushing force can be stated for AGL 1b. For AGL 2 with a higher particle size pressure plasticity e is at low densification higher and at high densification similar when compared with AGL 1a and b. Time plasticity d is higher at all $\rho_{rel,max}$ and ω is higher at low $\rho_{rel,max}$ and ω is similar at high $\rho_{rel,max}$. Elastic recovery of the tablets falls in between the products from manufacturer 1 and the crushing force is the lowest for this AGL. Finally, we will look at AGL 3, which has the highest particle size of all of the AGL we analyzed. Pressure plasticity e is at low densification equal to AGL 2, however at high densification it is lower; d at low densification is also equal to AGL 2, however, at high densification it is higher; and ω is, at all stages of densification, equal to AGL 1a. AGL 3 tablets show a high elastic recovery after tableting and the crushing force is the highest of all four AGL. A high particle size seems to be an advantage with regards to a high crushing force.

Fig. 3c exhibits the 3D parameter plots for the two LA, LA 1, and LA 3. Pressure plasticity e is higher at low densification for the material from manufacturer 1; at higher densification the e-values are more similar. Time plasticity d is generally higher for LA 3 when compared with LA 1, which means that LA 3 deforms faster. Finally, ω is lower at high $\rho_{rel,max}$ and higher at low $\rho_{rel,max}$. After tableting, LA 1 tablets exhibit a higher elastic recovery when compared with LA 3 tablets. The tablets crushing force for both LA is high. LA 3 tablets possess a slightly lower crushing force.

Fig. 3d exhibits the 3D parameter plots of three SL from three manufacturers. SL 1 and SL 2 have the same median particle size. The d- and e-values of both materials fall in between standard deviation, however, ω differs mainly at higher densification (ω is higher for SL 1). The compression behavior of SL 3 deviates in pressure plasticity e at higher densification from that of SL 1 and 2. The pressure plasticity e is lower for SL 3 and the material is thus less deformable. In addition the SL 3 material deforms slower (lower d-values) at low densification and faster (higher d-values) at high densification. This can be attributed to a slightly lower median particle size. Finally, ω is higher at low densification and thus SL 3 more plastic. After tableting, SL 1 tablets show higher elastic recovery and a lower crushing force. SL 2 and 3 tablets show the same elasticity after tableting, however, the crushing force is much higher for SL 3 tablets.
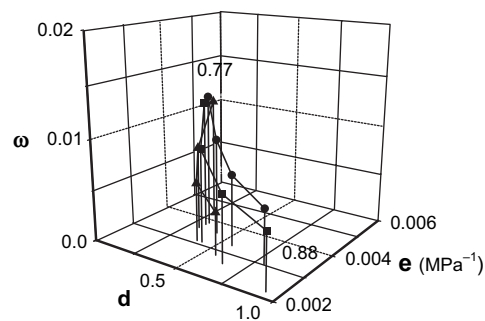
The results of this comparison show that particle size is not the only factor influencing deformation. Materials must have different surface properties which are responsible for different deformation and bonding. Furthermore, it can be concluded, that 3D modeling is able to distinguish the deformation behavior of materials which are only slightly different as those from different manufacturers.

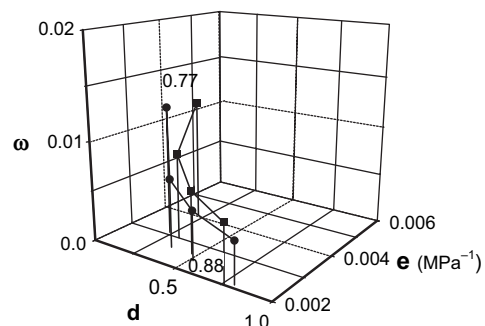## Final Formation of Lactose Tablets

In addition to the results mentioned above we have also determined that elastic recovery is dependent on time (Fig. 4). At first, the changes seemed to be neglectable, since for LA and LM no changes in tablet height could be determined, AGL showed a small peak, and for SL a slightly bigger peak could be determined. It was not possible to determine any differentiation among the materials from different
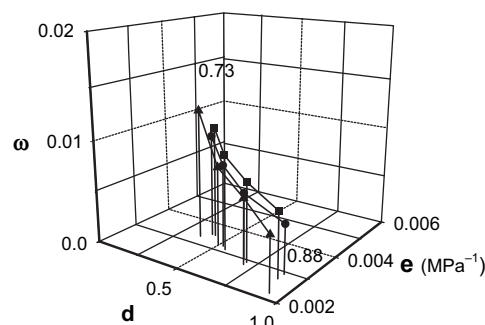
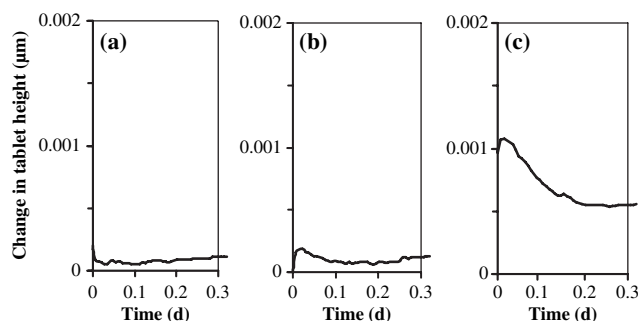*Lactoses by 3D Modeling and Fractal Analysis*

manufacturers. The results indicate that when expansion material changes take place this in turn causes a slight shrinking of the tablet. This shrinking could only be detected for the materials which have an amorphous content and it might be due to reorganization of the material structure (Picker, 2002). It could be related to a reversible exceeding of the T_g during tableting as mentioned above.

SEM Images: Visual Observation

The morphology of powders and tablets was analyzed by scanning electron microscopy.
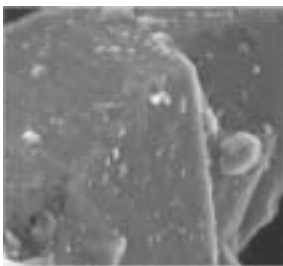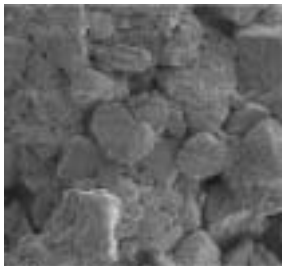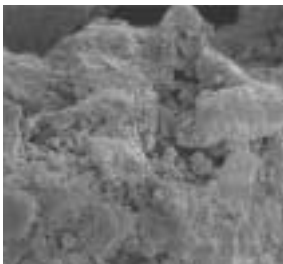
Typical SEM images (Table 3) of the different lactose powders show a similar, broken, non-organized and noncompacted structure. The surface of the powders was rather smooth, even when for LA, AGL, and SL agglomerates can be observed.

The SEM images of the surface of the lactose tablets show smooth surfaces of smashed lactose particles (Table 3) and that these lactose particles touch each other. Brittle fracture during compaction is the cause for this appearance. Differences for the different types of lactose are visible: AGL tablets exhibit a surface, which appears less smooth than that of the other materials. In this case, compression just produces an increase of contact area for bonding between the individual particles. For tablets produced from the other lactose types, a more homogeneous structure results. The SEM images exhibit not only differences among different types of lactose, due to pretreatment, but there are also differences among the materials from different manufacturers.

FIGURE 3 3D-Parameter Plot in Dependence on $\rho_{rel,\,max}$ (0.77–0.88) of Different Lactoses With Different Particles Sizes: (a) α-Lactose Monohydrate ■ 100 μm (LM 2a), ● 60 μm (LM 1), and ▲ 60 μm (LM 2b), (b), Agglomerated Lactose ■ 140 μm (AGL 3), ● 100 μm (AGL 2), ▲ 80 μm (AGL 1b), and □ 60 μm (AGL 1a), (c) Lactose Anhydrous ■ 150 μm (LA 1) and ● 150 μm (LA 3), and (d) Spray-Dried Lactose ■ 120 μm (SL 1), ● 120 μm (SL 2), and ▲ 110 μm (SL 3).
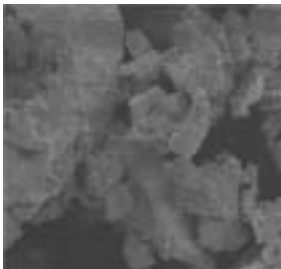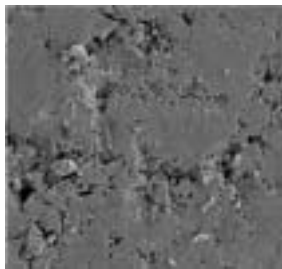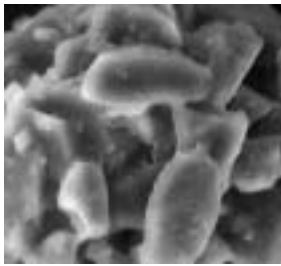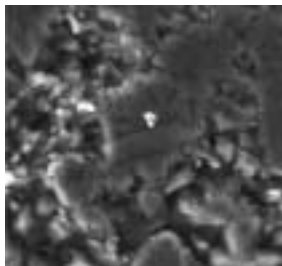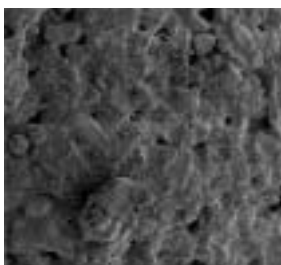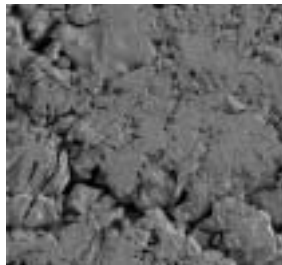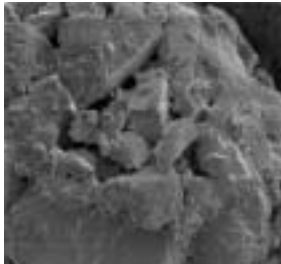
FIGURE 4 Change in Tablet Height Measured Exemplarily by TMA for Tablets Made From (a) α-Lactose Monohydrate, (b) Agglomerated Lactose, and (C) Spray-Dried Lactose. at a Maximum Relative Density of 0.85.

Z. Jelcic et al.

TABLE 3   SEM Pictures of the Surface of Lactose Powders and Tablets (1500×)

	Powder		Tablet	
	Original SEM image	Stentiford thinned SEM image	Original SEM image	Stentiford thinned SEM image
LM 1				
LM 2a				
AGL 2				
AGL 3				
LA 1				

(Continued)

Lactoses by 3D Modeling and Fractal Analysis

TABLE 3   *(Continued)*

	Powder		Tablet	
	Original SEM image	Stentiford thinned SEM image	Original SEM image	Stentiford thinned SEM image
LA 3				
SL 1				
SL 2				
SL 3				

The thinned images by Stentiford algorithm show a network-like structure that corresponds to surfaces of nonhomogenity or particles touching lines. For the tablets these distinctive structures are the result of mechanical treatment and determine tablet properties. However, it is clear that from observation alone heterogenity cannot be quantified. Thus, powder and tablet fractal indices were calculated and correlated with the powder, tableting and tablet properties. This allows for a quantitative analysis of lactose powder restructuring by following any changes in the fractal indices.

SEM Images: Fractal Analysis

Visually, SEM images with values of $D < 2$ exhibit heterogeneous, diffuse, and structureless patterns consistent with visualization of structural components within the lactose tablets. This can readily be seen by examining SEM images, where the patterns associated with anhydrous lactoses have a more granular texture

than that seen for SEM images of crystalline lactoses. The solid (D_{BBW}) and pore (D_{WBW}) mass fractal indices show a clear dependence on the lactose powder particle genesis. These differences are reflected in higher D-values for anhydrous lactose (average values $D_{BBW,powder} = 1.93 \pm 0.00$) versus crystalline lactoses (LM) (average values $D_{BBW,powder} = 1.96 \pm 0.02$). The tablet surface and pore fractal indices D_{BW} and D_{WBW} are statistically significant correlated to the corresponding powder fractal indices. However, the powder and tablet solid fractal indices D_{BBW} are not statistically significant correlated, mainly due to the fact that the tablet D_{BBW} indices have lost its informative power being almost constant for the various lactose tablets (in the range from 1.75 up to 1.9).

Two types of analysis were performed. First, each of the relations of interest was established for the lactose powders, the 3D-tableting parameters and the compacts, analyzed all together, and then, the same analysis was applied to the inverse problem, the determination of fractal indices from the 3D model parameters.

Powder Properties Correlation with Fractal Indices

In the following, the emphasis is on the details concerning the relation between some powder, tableting and tablet properties of the lactose, and the surface structure showed by fractal dimensions (Table 4).

The Carr's indices have already been discussed as given above; however, they can be also described by the powders' fractal indices. The classical solid box-counting $D_{BBW,powder}$ and void $D_{BBW,powder}$ fractal indices can describe flowability as determined by the Carr's index. This means that the powders fractality as exhibited by the powder surface, which was just spread on the SEM holder, also can represent the Carr's index, based on bulk and tap density. LA types that have a worse flowability, also, have (on the average) the lowest powder fractal indices $D_{BBW,powder}$.

Tableting Properties Correlation with Fractal Indices

The densification behavior of lactose by tableting was characterized by the three 3D-model parameters: time plasticity d, pressure plasticity e and the angle of torsion ω. Tableting properties, characterized by the 3D-model parameters, represent the "black box" connecting the powder and tablet properties/ structure. The fractal indices determined at the powder and tablet SEM images can describe the 3D-model tableting properties (Table 4).

The time plasticity d can be described by the statistically significant linear, bivariate relation with the solid $D_{BBW,tablet}$ mass fractal indices. The pressure plasticity e is well related with the linear combination of powder fractal indices ($D_{BW,powder}$ and $D_{BBW,powder}$). This entails that the powder structure determines the change in density (by pressure).

The pressure plasticity e, that describes the relationship between density and pressure, can also be described by a statistically significant linear combination of the tablet fractal indices $D_{BW,tablet}$, $D_{BBW,tablet}$, and $D_{WBW,tablet}$. This induces that the change in density is related to the tablet fractal indices. The pressure plasticity e increases in the following order: LA $<$ SL $\leq$ AGL $<$ LM. The corresponding series is observed for the surface fractal index $D_{BW,powder}$: LA (1.755 $\pm$ 0.087) $<$ SL (1.806 $\pm$ 0.210) $\leq$ AGL (1.852 $\pm$ 0.011) $<$ LM (1.778 $\pm$ 0.222).

The angle of torsion ω is a measure of the material's elasticity. When fast elastic decompression indicated by ω increases, elasticity decreases. The fast elastic decompression ω can be well described by a single, surface tablet fractal index, $D_{BW,tablet}$ The fast elastic decompression is best described from all of the three 3D-model parameters, by the powder fractal indices linear combination ($D_{BW,powder}$ and $D_{BBW,powder}$).

The results of the fractal analysis were linked to the 3D-model tableting properties of the lactose from which the tablets were compressed. The single tableting 3D-model parameters can be well described by the linear combination of tablets' fractal indices. Specifically, the pressure plasticity e and the elastic decompression ω can well be described by the linear combination of powders' fractal indices. As already discussed LM presents a material with brittle fracture. For AGL and for LA and SL less fracture and a more homogenous deformation mechanism is observed. Thus, the brittle fracture decreases as follows: LM $>$ AGL $>$ LA $>$ SL. This is in accordance with the average surface fractal indices $D_{BW,tablet}$: LM (1.622 $\pm$ 0.265) $<$ AGL (1.736 $\pm$ 0.124) $<$ LA (1.766 $\pm$ 0.219) $<$ SL (1.794 $\pm$

Lactoses by 3D Modeling and Fractal Analysis

TABLE 4 Linear Regression of Tablet and Powder Properties, and Tableting 3D-Model Parameters with the Fractal Indices by the Box-Counting Method

Property	Model equation	$|R|$	R^2 (%)	R^2, adj.	F_{signif} $(k, n-k-1)$
From original SEM powder images					
Carr-index	$= 53325.1 + 2056.6 \times D_{BW,powder} - 28619.4 \times D_{BBW,powder} - 27502.7 \times D_{WBW,powder}$ $- 890.5 \times D_{BW,powder} \times D_{WBW,powder} + 14596.5 \times D_{BBW,powder} \times D_{WBW,powder}$	0.959 ($p = 0.05$)	92.08	0.787	F_{signif} (5,3) = 0.07 (<0.10)
e	$= 0.01212 - 0.05022 \times D_{BW,powder} + 0.02301 \times D_{BW,powder} \times D_{BBW,powder}$	0.779 ($p = 0.05$)	60.7	0.477	F_{signif} (2,6) = 0.06 (<0.10)
ω	$= -0.08923 - 0.01026 \times D_{BW, powder} + 0.05788 \times D_{BBW,powder}$	0.890 ($p = 0.05$)	79.3	0.724	F_{signif} (2,6) = 0.008 (<0.05)
Crushing strength (N)	$= -909.3 + 5285.2 \times D_{BW,powder} - 2415.8 \times D_{BW,powder} \times D_{BBW,powder}$	0.850 ($p = 0.05$)	72.3	0.631	F_{signif} (2,6) = 0.02 (<0.05)
From Stentiford thinned SEM powder images					
Carr-index	$= 60328.1 - 26709.6 \times D_{BW, Stentiford,powder} - 30309.0 \times D_{WBW,Stentiford,powder}$ $- 116.65 \times D_{BW, Stentiford,powder} \times D_{BBW, Stentiford,powder} + 13538.5 \times$ $D_{BW, Stentiford,powder} \times D_{WBW,Stentiford,powder}$	0.978 ($p = 0.05$)	95.7	0.915	F_{signif} (4,4) = 0.005 (<0.05)
e	$= 0.04325 - 0.0458 \times D_{BW,Stentiford,powder} + 0.01321 \times D_{BW,Stentiford,powder} \times$ $D_{BBW,tentiford,powder}$	0.851 ($p = 0.05$)	72.4	0.632	F_{signif} (2,6) = 0.02 (<0.05)
Crushing strength (N)	$= -5171.7 - 665977.71 \times D_{BW,Stentiford,powder} + 6799864.4 \times D_{BBW,Stentiford,powder}$ $- 1487.4 \times D_{BW, Stentiford,powder} \times D_{BBW,Stentiford,powder} + 3334318.1 \times$ $D_{BW, Stentiford,powder} \times D_{WBW,Stentiford,powder} - 3404602.8 \times D_{BBW, Stentiford,powder} \times$ $D_{WBW,,Stentiford,powder}$	0.993 ($p = 0.05$)	98.5	0.960	F_{signif} (5,3) = 0.006 (<0.05)
Elastic recovery, ER (%)	$= 35.11 - 39.44 \times D_{BBW,Stentiford,powder} + 11.62 \times D_{BW,Stentiford,powder} \times D_{BBW,Stentiford,powder}$	0.838 ($p = 0.05$)	70.3	0.604	F_{signif} (2,6) = 0.02 (<0.05)
From original SEM tablets images					
Carr-index	$= 5.943 + 568.29 \times D_{BW,tablet} - 208.56 \times D_{BBW,tablet} - 179.32* D_{BW,tablet} \times D_{WBW,tablet}$	0.994 ($p = 0.05$)	98.7	0.978	F_{signif} (3,4) = 0.0002 (<0.05)
d	$= 1.599 - 0.413 \times D_{BBW,tablet}$	0.802 ($p = 0.05$)	64.4	0.584	F_{signif} (1,6) = 0.01 (<0.05)
e	$= -0.12 + 0.09102 \times D_{BBW,tablet} - 0.03744 \times D_{BW,tablet} \times D_{BBW,tablet} + 0.02249 \times D_{BW,tablet} \times$ $D_{WBW,tablet}$	0.928 ($p = 0.05$)	86.2	0.758	F_{signif} (3,4) = 0.03 (<0.05)
ω	$= 1.599 - 0.413 \times D_{BW,tablet}$	0.707 ($p = 0.05$)	50.1	0.417	F_{signif} (1,6) = 0.04 (<0.05)
Crushing strength (N)	$= 11938.4 - 8798.6 \times D_{BBW,tablet} + 3649.6 \times D_{BW,tablet} \times D_{BBW,tablet} - 2205.4 \times D_{BW,tablet} \times$ $D_{WBW,tablet}$	0.885 ($p = 0.05$)	78.4	0.621	F_{signif} (3,4) = 0.08 (<0.10)

*$|R|$ Coefficient of multiple correlation; R^2 (%) Coefficient of determination; R^2, adj. Coefficient of determination R^2, adjusted for df; $F_{signif}(k,n-k-1)$ Overall regression model significance.

0.172). The bivariate relations of the time plasticity d (with the tablet solid mass fractal index $D_{BBW,tablet}$) and the elastic decompression, the inverse of ω?(with the tablet surface fractal index $D_{BW,tablet}$) show underlying mechanism of the morphology genesis.

Most of the SEM imagined lactose tablets exhibit a pronounced rough structure. The extent of roughness appeared to be dependent on the compaction behavior of the lactose type and moreover, on the production method. Since there is a linear correlation between compression behavior and roughness for the twelve different materials, not only the type of lactose is decisive but also the special material with its own production method.

Tablet Properties Correlation with Fractal Indices

The elastic recovery is related to the linear combination of the powder fractal indices from the Stentiford thinned images (Table 4). This relation entails that the fractal roughness of the powder does not determine the elastic recovery. This can be ascribed to the obvious "network-like" powder thinned outline structure that is preserved in the tablet and which participates in the elastic response. The powder surface fractal index $D_{BW,powder,Stentiford}$ has a positive component effect, and the classical box-counting solid $D_{BBW,powder,Stentiford}$ fractal index has a negative component effect on the elastic recovery. The thinned images of LM1 and LA1, which have the largest elastic recovery, have more opened structures that are described by the lower values of the fractal index D_{BW}. The tablet fractal indices can not describe the elastic recovery. Furthermore, the elastic recovery of the lactose could not very well be related to the 3D modeling parameters. Only the elastic decompression, the inverse of ω indicates some kind of positive correlation with the elastic recovery, but this is, also, without statistical significance.

The strength of a compact is a function both of the intrinsic properties of the material and of extrinsic factors, which operate during compacting, handling and storage. The latter factors can be derived from the statistically significant linear relation of the crushing force and the pressure plasticity e. It is further substantiated by the fact that the pressure plasticity e corre-

lates well with the microhardness (Picker, 2002). The crushing force is statistically significant described by the linear combination of tablet fractal indices (Table 4). However, a good relation is also given by linear combination of powder fractal indices $D_{BW,powder}$ and $D_{BBW,powder}$ (Fig. 5). The powder classical solid box-counting $D_{BBW,powder}$ indices have a negative component effect, and the void $D_{WBW,powder}$ fractal indices have a positive component effect on the crushing force. The crushing force is rather well described even by the powder fractal indices derived from the Stentiford thinned images.

It is astonishing that the powder texture (as measured by the powder fractal indices) can determine the crushing force better than the tablets' surface texture (statistically significant for powder versus non-significant for tablet fractal indices). This might be due to the ability of the linear combination of powder fractal indices to properly describe the pressure plasticity e that is well related to the crushing force. The crushing force is improved by the increase in the powder surface $D_{BW,powder}$ fractal indices. Lactose compacts (Bolhuis & Chowhan, 1996) are consolidated by both plastic deformation and fragmentation, but largely by fragmentation. Fragmentation creates a large number of contact points that support the applied load, so that stress on each contact point is relatively small. Therefore, the strength of the bonds that form will be relatively weak (Bolhuis & Chowhan, 1996).
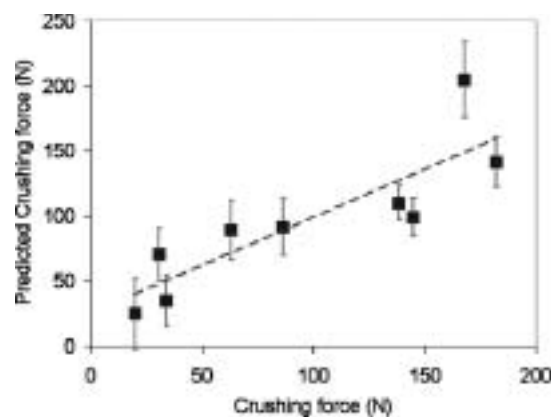
FIGURE 5   Linear Relation of Crushing Force and Predicted Crushing Force by Powder Fractal Indices $D_{BBW,powder}$ and $D_{WBW,powder}$; $R^2 = 0.741$.

Lactoses by 3D Modeling and Fractal Analysis

TABLE 5 Linear Regression of the Fractal Indices by the Box-Counting Methodology and the Tableting 3D-Model Parameters (an Inverse Problem)

Fractal index	Model equation	$\lvert R \rvert$	R^2 (%)	R^2, adj.	F_{signif} (k, $n-k-1$)
From original SEM powder images					
$D_{BW,powder}$	$= 1.32 + 499.07 \times e - 57979.2 \times e \times \omega$	0.725 ($p = 0.05$)	52.6	0.367	F_{signif} (2,6) = 0.10 (<0.10)
$D_{WBW,powder}$	$= 1.705 + 207.93 \times e - 26423.7 \times e \times \omega$	0.752 ($p = 0.05$)	56.5	0.420	F_{signif} (2,6) = 0.08 (<0.10)
From Stentiford thinned SEM powder images					
$D_{BW,Stentiford,powder}$	$= 1.231 + 611.69 \times e - 74780.5 \times e \times \omega$	0.747 ($p = 0.05$)	55.8	0.411	F_{signif} (2,6) = 0.08 (<0.10)
$D_{BBW,Stentiford,powder}$	$= 1.120 + 662.78 \times e - 79995.8 \times e \times \omega$	0.761 ($p = 0.05$)	57.9	0.438	F_{signif} (2,6) = 0.07 (<0.10)
$D_{WBW,Stentiford,powder}$	$= 2.026 - 9.135 \times \omega - 18.3 \times e \times d + 7.16 \times d \times \omega + 1975.3 \times e \times \omega$	0.972 ($p = 0.05$)	94.5	0.890	F_{signif} (4,4) = 0.008 (<0.05)
From original SEM tablets images					
$D_{BW, tablet}$	$= 1.071 + 727.11 \times e - 88205.3 \times e \times \omega$	0.930 ($p = 0.05$)	86.4	0.810	F_{signif} (2,5) = 0.006 (<0.05)
$D_{BBW, tablet}$	$= 3.15 - 1.56 \times d$	0.802 ($p = 0.05$)	64.4	0.584	F_{signif} (1,6) = 0.01 (<0.05)
$D_{WBW, tablet}$	$= 1.523 + 509.46 \times e \times d - 52673.4 \times e \times \omega$	0.788 ($p = 0.05$)	62.0	0.468	F_{signif} (2,5) = 0.08 (<0.10)
From Stentiford thinned SEM tablets images					
$D_{BW,Stentiford,tablet}$	$= 12.25 - 12.47 \times d - 1015.9 \times e - 1565.1 \times \omega + 1575.2 \times d \times e + 1671.6 \times d \times \omega$	0.999 ($p = 0.05$)	99.7	0.992	F_{signif} (5,3) = 0.0005(<0.05)
$D_{BBW,Stentiford,tablet}$	$= 12.10 - 12.33 \times d - 822.53 \times e - 1638.4 \times \omega + 1362.2 \times d \times e + 1744.1 \times d \times \omega$	0.998 ($p = 0.05$)	99.7	0.992	F_{signif} (5,3) = 0.0005 (<0.05)
$D_{WBW,Stentiford,tablet}$	$= 1.961 + 0.0449 \times d + 13.87 \times e + 0.505 \times \omega - 17.95 \times d \times e$	0.965 ($p = 0.05$)	93.1	0.861	F_{signif} (4,4) = 0.01 (<0.05)

*$\lvert R \rvert$ Coefficient of multiple correlation; R^2 (%) Coefficient of determination; R^2, adj. Coefficient of determination R^2, adjusted for df; F_{signif} (k, $n-k-1$) Overall regression model significa.

Inverse Problem: Fractal Indices from the 3D-Model Parameters

Some of the powder and the tablet fractal indices (and some fractal indices determined from Stentiford thinned SEM images) can be described by the linear combination of the 3D-model parameters. This can be useful for finding the appropriate compact morphology (measured by the fractal indices) that is suitable for controlling the rate of drug release of dissolution-controlled systems (Table 5).

The surface $D_{BW,powder}$ and void $D_{WBW,powder}$ fractal indices are well related to the fast elastic decompression ω and the pressure plasticity e. The solid powder fractal indices $D_{BBW,powder}$ are not statistically significant related to the 3D-model parameters. There is a statistically significant linear relation of the tablet, surface fractal index $D_{BW,tablet}$ with the pair of 3D-model parameters, the pressure plasticity e and the fast elastic decompression, the inverse of ω. The classical box-counting solid fractal index $D_{BBW,tablet}$ is linearly (bivariate) related to the time plasticity d. The statistically nonsignificant linear relation with the fast elastic decompression, the inverse of ω is observed for the pore fractal index $D_{WBW,tablet}$.

From a theoretical point of view, the larger the solid fractal dimension the higher is the solid occupied space, and as a consequence the larger the bulk density. This conclusion agrees with general assessments about the solid set mass fractal dimension dynamics. The solid mass fractal dimensions D_{BBW} should be higher and the pore mass fractal dimensions D_{WBW} lower for the more compacted tablets. Therefore, the D_{BBW} is inversely related to average porosity.

The fractal indices from the Stentiford thinned SEM tablet images, such as the classical box-counting fractal index $D_{BBW,Stentiford,tablet}$ the surface fractal index $D_{BW,Stentiford,tablet}$, and the pore fractal index $D_{WBW,Stentiford,tablet}$ can be related to the 3D-model

parameters: the pressure plasticity e and the fast elastic decompression ω.

These results imply that the fractal indices can be described by the 3D-model tableting parameters. Concerning the tablets' indices, it might be obvious that the tableting performance can lead to the specific morphology as seen by SEM and indexed by fractal analysis. The solid, classical box-counting, solid fractal index $D_{BBW,tablet}$ is determined by the time plasticity d, and the surface fractal index $D_{BW,tablet}$ is a linear function of the pressure plasticity e, and the elastic decompression ω. The morphology genesis can be followed by following the 3D-model parameters. However, the inverse problem with the powders' fractal indices might not be so obvious (strong, but statistically nonsignificant relationship). However, the morphology roughness observed in powders and on tablets' surfaces are strongly correlated which is due to morphology preservation in lactose compaction. The accuracy of the skeleton extraction method by thinning directly affects the accuracy of the fractal dimension computation. The thinned SEM images represent the true skeletal structure with satisfactory accuracy. However, the generated skeleton was rather "empty" in some areas for LM1, LA1, and SL1. This may influence the fractal dimension calculation of thinned images since the box-counting dimension needs a certain pixel coverage level for accurate calculation. Therefore, it may be necessary to evaluate the fractal properties of excipient thinned structure, especially those of high complexity such as the particle and compacts, from different aspects to make a more comprehensive understanding.

CONCLUSION

The results show that 3D modeling can precisely distinguish the deformation behavior of only slightly different materials. The time plasticity d, the pressure plasticity e, and the angle of torsion ω as a measure for the materials elasticity give valuable information on the distinct excipient. A differentiation is possible to establish not only for different types of lactose, but also for the same type of lactose that is produced by different manufacturers.

The fractal dimensions of solid and pore networks are useful parameters capable of distinguishing between materials with different production genesis. The solid mass fractal dimension near 2, and the pore mass fractal dimension near 1.8, may be proposed as the bounded values for the lactose solid and pore networks. The pore mass fractal dimension D_{WBW} reflects the compaction status, the solid mass fractal dimension D_{BBW} depends more on material genesis.

The effect of the production method on the fractal dimensions D_{BW}, D_{BBW}, and D_{WBW} was proved by analysis of variance. The fractal D values can provide a better understanding of the genesis processes behind the formation of any given structure.

Furthermore, it is possible to establish simple and statistically coherent relations between fractal parameters and some physical properties of powders and tablets. Fractal analysis showed that the 3D-model parameters can be described by fractal indices as obtained from SEM images. However, the inverse is also possible; fractal indices can be described by the 3D-model parameters.

In conclusion, 3D-model parameters are strongly connected to the morphology of the tablet and they not only provide information on tableting characteristics but also on the final tablet morphological properties.

REFERENCES

Ahammer, H., & DeVaney, T. T. J. (2004). The influence of edge detection algorithms on the estimation of the fractal dimension of binary digital images. *Chaos: An Interdisciplinary J. of Nonlinear Sci., 14*(1), 183–188.

Armstrong, N. A., & Haines-Nutt, R. F. (1972). Elastic recovery and surface area changes in compacted powder systems. *J. Pharm. Pharmacol., 24S*, 135P–136P.

Avnir, D., Farin, D., & Pfeifer, P. (1984). Molecular fractal surfaces. *Nature, 308*, 261–263.

Blacher, S., Henrioulle, N., Brouers, F., & Sarychev, A. (1997). Scaling properties of complex gray level images. *Acta Stereol., 16*, 19–29.

Bolhuis, G. K., & Chowhan, Z. T. (1996). Materials for direct compaction. In *Pharmaceutical powder compaction technology*, Alderborn, G., Nyström, C., Eds., Marcel Dekker: New York, 419–500.

Bolhuis, G. K., Reichman, G., Lerk, C. F., van Kamp, H. V., & Zuurman, K. (1985). Evaluation of anhydrous alpha-lactose, a new excipient in direct compression. *Drug Dev. Ind. Pharm., 11*, 1657–1681.

Bower, Ch., Washington, C., & Purewal, T. S. (1995). Fractal morphology of drug aggregates in aerosol propellant suspensions. *Int. J. Pharm., 118*, 229–235.

Buchníček, M., Nežádal, M., & Zmeškal, O. (2000). Numeric calculation of fractal dimension. In *Nostradamus, Prediction Conference*, FT VUT: Zlin.

Busignies, V., Tchoreloff, P., Leclerc, B., Besnard, M., & Couarraze, G. (2004). Compaction of crystallographic forms of pharmaceutical granular lactoses. I. Compressibility. *Eur. J. Pharm. Biopharm., 58*(3), 569–576.

Carr, R. L. (1965). Evaluating flow properties of solids. *Chem. Eng., 72*, 163–168.

Chappard, D., Degasne, I., Huré, G., Legrand, E., Audran, M., & Baslé, M. F. (2003). Image analysis measurements of roughness by texture and fractal analysis correlate with contact profilometry. *Biomaterials, 24*, 1399–1407.

Concessio, N. M., & Hickey, A. J. (1997). Descriptors of irregular particle morphology and properties. *Adv. Drug Del. Rev., 26*, 29–40.

Ferrari, F., Cocconi, D., Bettini, R., Giordano, F., Santi, P., Tobyn, M., Price, R, Young, P, Caramella, C., & Colombo, P. (2004). The surface roughness of lactose particles can be modulated by wet-smoothing using a high-shear mixer. *AAPS PharmSciTech., 5*(4): article 60.

Fini, A., Fazio, G., Fernandez-Hervas, M. J., Holgado, M. A., & Rabasco, A. M. (1996). Fractal analysis of sodium cholate particles. *Pharm. Sci., 85*(9), 971–975.

Fini, A., Fernandez-Hervas, M. J., Holgado, M. A., Rodriguez, L., Cavallari, C., Passerini, N., & Caputo, O. (1997). Fractal analysis of beta-cyclodextrin-indomethacin particles compacted by ultrasound. *J. Pharm. Sci., 86*(11), 1303–1309.

Frame, M., Mandelbrot, B., & Neger, N. (2006). *Fractal Geometry*. http://classes.yale.edu/fractals/, accessed on 7/5/2006.

Gunsel, W. C., & Lachman, L. (1963). Comparative evaluation of tablet formulations prepared from conventionally processed and spray-dried lactose. *J. Pharm. Sci., 52*, 178–182.

Hanus, E. J., & King, L. D. (1968). Thermodynamic effects in compression of solids. *J. Pharm. Sci., 57*, 677–684.

Heckel, R. W. (1961). Density-pressure relationships in powder compaction. *Trans Metall. Soc. AIME, 221*, 671–675.

Hickey, A. J., & Concessio, N. M. (1994). Flow properties of selected pharmaceutical powders from a vibrating spatula. *Part. Part. Syst. Charact., 11*, 457–462.

Holgado, M. A., Fernández-Hervás, M. J., Fernández-Arévalo, M., & Rabasco, A. M. (1995). Use of fractal dimensions in the study of excipients: application to the characterization of modified lactoses. *Int. J. Pharm., 121*, 187–193.

Kaye, B. H. (1995). Applied fractal geometry and powder technology. *Chaos, Solitons & Fractals, 6*, 245–253.

Khan, H., Fell, J. T., & Macleod, G. S. (2001). The influence of additives on the spreading coefficient and adhesion of a film coating formulation to a model tablet surface. *Int. J. Pharm., 227*, 113–119.

Lerk, C. F. (1993). Consolidation and compaction of lactose. *Drug Dev. Ind. Pharm., 19*, 2359–2398.

Mandelbrot, B. B. (1982). *The Fractal Geometry of Nature*. W. H. Freeman and Company: New York.

Narayan, P., & Hancock, B. C. (2005). The influence of particle size on the surface roughness of pharmaceutical excipient compacts. *Mater. Sci. Eng. A, 407*, 226–233.

Picker, K. M. (2000). A new theoretical model to characterize the densification behavior of tableting materials. *Eur. J. Pharm. Biopharm., 49*(3), 267–273.

Picker, K. M. (2002). *New insights in the process of tablet formation – Ways to explore soft tableting*. Habilitation thesis [Habilitationsschrift]. Halle, Germany, Martin-Luther-University Halle-Wittenberg and Görich und Weiershäuser Verlag, Marburg.

Picker, K. M. (2003a). The 3-D model: comparison of parameters obtained from and by simulating different tabletting machines. *AAPS PharmSciTech., 4*(3), article 35.

Picker, K. M. (2003b). The 3-D model: does time plasticity represent the influence of tabletting speed? *AAPS PharmSciTech., 4*(4), article 66.

Picker K. M. (2003c). The relevance of glass transition temperature for the process of tablet formation. *J. Therm. Anal. Cal., 73*(2), 597–605.

Picker, K. M. (2004). The 3D model: Explaining densification and deformation mechanisms by using 3D parameter plots. *Drug Dev. Ind. Pharm., 30*(4), 413–425.

Picker, K. M., & Bikane, F. (2001). An evaluation of three-dimensional modeling of compaction cycles by analyzing the densification behavior of binary and ternary mixtures. *Pharm. Dev. Technol., 6*(3), 333–342.

Picker-Freyer, K. M., & Schmidt, A. G. (2004). Does temperature increase induced by tableting contribute to tablet quality? *J. Therm. Anal. Cal., 77*, 531–539.

Podczeck, F. (1998). Measurement of surface roughness of tablets made from polyethylene glycol powders of various molecular weights. *Pharm. Pharmacol. Commun., 4*, 179–182.

Podczeck F., Brown, S., & Newton, J. M. (1999). The influence of powder properties and tabletting conditions on the surface roughness of tablets. *Part. Part. Syst. Charact., 16*(4), 185–190.

Riippi, M., Antikainen, O., Niskanen, T., & Yliruusi, J. (1998). The effect of compression force on surface structure, crushing strength, friability and disintegration time of erythromycin acistrate tablets. *Eur. J. Pharm. Biopharm., 46*, 339–345.

Rowe, R. C. (1979). Surface roughness measurements on both uncoated and film-coated tablets. *J. Pharm. Pharmacol., 31*(7), 473–474.

Schmidt, J. (1997). Direkttablettierung niedrigschmelzender nichtsteroidaler Antirheumatika mit mikrokristallinen Cellulosen. PhD thesis, Martin-Luther-Universität Halle-Wittenberg.

Sebhatu, T., Ahlneck, C., & Alderborn, G. (1997). The effect of moisture content on the compression and bond-formation properties of amorphous lactose particles. *Int. J. Pharm., 146*, 101–114.

Seitavuopio, P., Rantanen, J., & Yliruusi, J. (2003). Tablet surface characterization by various imaging techniques. *Int. J. Pharm., 254*(2), 281–286.

Seitavuopio, P., Rantanen, J., & Yliruusi, J. (2005). Use of roughness maps in visualisation of surfaces. *Eur. J. Pharm. Biopharm., 59*(2), 351–358.

Stentiford, F. W. M., & Mortimer, R. G. (1983). Some new heuristics for thinning binary handprinted characters for OCR. *IEEE Transactions on Systems, Man, and Cybernetics, 13*(1), 81–84.

Tang, P., Chan, H-K., & Raper, J. A. (2004). Fractal Geometry in Pharmaceutical and Biological Applications – A Review. In *Encyclopedia of Pharmaceutical Technology (Third Edition)*. Published online May 11, 2004, 1–16. www.dekker.com, accessed on 7/5/2006.

Underwood, E. E., & Banerji, K. (1983). Statistical analysis of facets in a computer simulated surface. *Acta Stereol., 2S1*, 75–80.

Vromans, H., Bolhuis, G. K., Lerk, C. F., van de Biggelaar, H., & Bosch, H. (1987). Studies on tableting properties of lactose. VII. The effect of variations in primary particle size and percentage of amorphous lactose in spray-dried lactose products. *Int. J. Pharm., 35*, 29–37.